KONVERSI

Chemical and physical activation of natural pyrite as potential inorganic pigment material

Rendy Muhamad Iqbal[1,2,3,*], Sari Namarito Simarmata[1], Tiara Cristy Sinaga[1], Elfrida Roulina Simanjuntak[1], Riandy Putra[1], Deni Shidqi Khaerudini[4]

[1]*Department of Chemistry, Faculty of Mathematics and Natural Sciences, Universitas Palangka Raya, Palangka Raya 73111, Indonesia*
[2]*Department of Chemistry, Faculty of Science, Universiti Teknologi Malaysia, Skudai 81310, Johor, Malaysia*
[3]*Advanced Membrane Technology Research Centre (AMTEC), Faculty of Chemical and Energy Engineering, Universiti Teknologi Malaysia, Skudai 81310, Johor, Malaysia*
[4]*Research Centre for Advanced Material, National Research and Innovation Agency (BRIN), South Tangerang, Banten 15314, Indonesia*

ARTICLE INFO	ABSTRACT
	Pyrite is one of the minerals on Borneo Island. It has a disadvantage for soil quality due to its acidic properties. One of the main components of pyrite is iron, which promises to be utilized as an inorganic pigment. This research aims to transform pyrite into red-brown pigment material-based iron oxide. Based on the XRF result, the highest component is Fe, with a percentage up to 42%. This data is also suitable for an iron oxide phase from the diffractogram of pigment, followed by the presence of silica and alumina structures. The physical activation process successfully transformed the color of the of the materials from gold to red-brown. Then, the molecular vibration of Fe–O also appears on FTIR spectra at a wavenumber of 483 cm^{-1} and T–O–T bending at 994 cm^{-1}. Moreover, morphological observation exhibits the aggregation of particles and the distribution of iron elements on the entire area of pigment surface. Based on the above findings, it can be concluded that pyrite minerals can be transformed into hematite-based red pigment, which is promising to be utilized in the painting sector.

1. Introduction

Indonesia is a country that has a wealth of scattered and various types of geological resources, one of which is pyrite. Pyrite is one type of heavy and conductive material. The chemical composition found in pyrite (FeS$_2$) is 46% of Fe and 53.4% of S content, and minor component such as Co, As, Sb, Cu, Au, and Ag [1]. Pyrite distribution can be related to coal distribution because pyrite minerals are typically concentrated in coal deposits. It means that the distribution of coal mining in Indonesia was indicated by pyrite near coal mine locations. It was fascinating because Indonesia has a large amount of coal mining and still uses the coal power plant as the primary source of electricity production [2,3].

On the other hand, acid sulfate soil is found in some locations, such as Borneo Island, containing pyrite [4]. In Borneo Island, pyrite coexists with peat, where peat soil formed in a marine environment has a soil layer containing sulfidic material (pyrite: FeS$_2$). If it oxidized, it will create a sulfuric horizon. One of the most destructive soil properties in swamps is formed by deposition in areas affected by sea or peat tides [5]. Based on distribution, the area soil contained pyrite in Borneo around 259,424 ha (32.19%) [4]. Nevertheless, the pyrite mineral, which is still considered one of the scourges of problems in agricultural processing, because the release of S

element can increase soil acidity while it oxidized sulphate.

Pyrite minerals are also deposited in nature together with aluminosilicate minerals, it depends on the origin of the mineral formation [4]. Pyrite contains a high amount of iron that can be utilized in many sectors. Iron-based materials have been used as photoanode materials [6,3], magnetic adsorbents [7], magnetic materials [8], heterogeneous catalysts and photocatalysts [9], precursors for the synthesis of perovskite and fluorite (advanced materials) [10,11,12,13,14], and many more.

Another promising iron-based material is inorganic-based pigment material. He et al. [15] reported that pyrite contains iron, which has the potential to be transformed into a red-brown pigment. Tamura et al. [16] explained that red pigment could be formed from hematite or iron mixed with other compounds, which have the potential to be explored from natural minerals. Recently, there have been limited reports about the prospect of pyrite and its characteristics as a candidate material for inorganic pigments. The pyrite mineral can be processed using several techniques, such as physical and chemical processing. The using heat exposure or ball milling was categorized as physical treatment [17]. Then, acid or base activation was introduced as a chemical activation for mineral processing [17].

Therefore, this study aims to observe the effect of chemical and physical activation of the pyrite mineral to obtain red pigments based on inorganic natural materials in an effort to explore and utilize minerals in Indonesia. Activation is intended to remove some impurities and increase the color intensity of the pigments formed.

* Corresponding author. Tel.: +628113238685
Email: iqbal.rm@mipa.upr.ac.id

2. Materials and Methods

2.1. Materials

Pyrite minerals have been sampled from Garong Village (Pulang Pisau Regency, Central Borneo Province, Indonesia), Sodium hydroxide (Aldrich, 98%), and distilled water.

2.2. Activation of natural pyrite

The activation of natural pyrite was followed by two mechanisms: chemical activation *via* KOH immersion, followed by physical activation using heat treatment. The pyrite sample was dried at 110 °C for 3 hours to remove the water content and ground into fine particles; then, the fine particles were immersed in KOH 1 M for 60 minutes and continued the drying process to complete the chemical activation process. Afterward, 25 grams of the treated sample were calcined at 800 °C with various calcination times for 1, 2, and 3 hours (samples were denoted as 1 h, 2 h, and 3 h).

The sample characterization was carried out using X-Ray Fluorescence (XRF) PANanalytical Minipal 4 to determine the chemical composition, X-Ray Diffraction (XRD) PANanalytical Expert Pro for structural analysis, the Fourier-Transform Infrared (FTIR) Spectrophotometer Shimadzu 84000S was used for functional group analysis, the Field Emission-Scanning Electron Microscope (FE-SEM) FEI Quanta FEG 650 was used for morphological observation of the sample, and energy dispersive X-ray was used to determine the element in the pigment sample.

3. Results and Discussion

3.1. XRF analysis

XRF characterization was used to determine the chemical composition of the initial and treated natural pyrite. As shown in Figure 1, the Fe content has a higher composition, followed by Si, Al, Ti, and K. Si and Al were also detected as the second and third most significant compositions due to the iron also deposited together with the aluminosilicate-based mineral during the mineral formation. The Fe content reaches up to 47.67% for the initial sample, then 33.6% and 13% for Si and Al, respectively. The chemical activation result is also represented in Figure 1; most of the content was decreased after the base activation, but the K content was increased due to the K from the base activator attached to the surface of the particles, which is the reason for the higher K content after chemical activation. All elements can be dissolved in a base condition or in a in a base solvent. The Fe content still has the highest concentration for the composition, which means it can be used as a red pigment. However, other elements like Si, Al, Ti, and K exist in the sample.

3.2. Structural analysis and crystallite size determination

X-ray diffraction (XRD) was used to conduct the structural investigation, as illustrated in Figure 2. The quartz structure (SiO_2) was indicated by the peaks on 2θ of 20.98° (1 0 0) and 26.79° (1 0 1) [18]. Following chemical activation, the peaks at 36.6° and 37.01° still show pyrite structure. The occurrence of many peaks on 2θ at 33.57°, 34.8°, 50.2°, 60.4°,

and 68.25°, which were connected to the crystal structure of Fe_2O_3 demonstrated the phase transformation from pyrite to hematite [19,20]. According to Li et al. [21], small peaks at an angle of 40 to 45° were predicted to show the presence of the Al_2O_3 phase or diffraction from the aluminosilicate building unit. Besides that, the physical activation successfully changed the color of the pigmenting material from gold to red-brown with various calcination times, as shown in Figure 3.
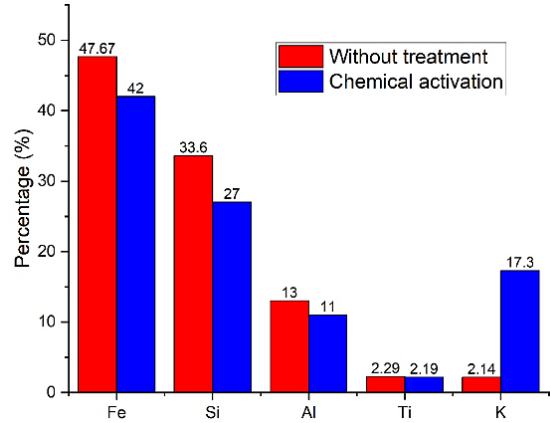

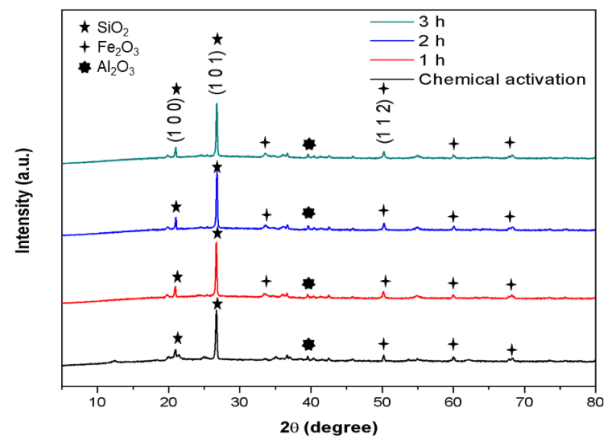Fig. 1. The chemical composition of initial and chemical activation of natural pyrite

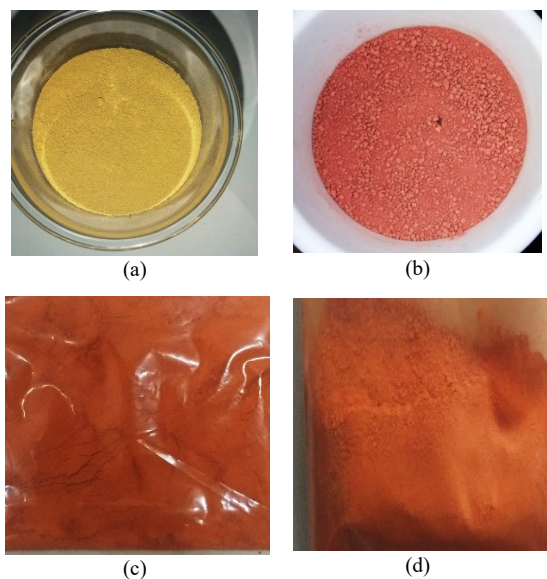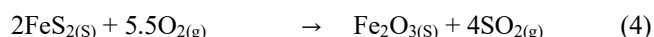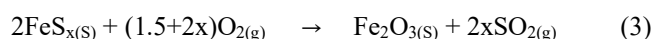Fig. 2. Diffractogram of initial and treated natural pyrite

Fig. 3. Colors transformation of pyrite: (a) chemical activation, (b) 1 hour, (c) 2 hours, and (d) 3 hours of calcination duration

The components in pigment materials underwent a phase shift, as seen by the color variation brought about by the activation process. The element was successfully converted into metal oxide throughout the heating process in an oxygen-rich environment, despite the fact that the original sample undergoing chemical activation may have been complex for the oxidized metal components. Equations 1-4 describe the reactions that lead to the conversion of the pyrite structure into iron oxide.

$$FeS_{2(S)} \rightarrow FeS_{x(S)} + (1{-}0.5x)S_{2(g)} \quad (1)$$

$$S_{2(g)} + 2O_{2(g)} \rightarrow 2SO_{2(g)} \quad (2)$$

$$2FeS_{x(S)} + (1.5{+}2x)O_{2(g)} \rightarrow Fe_2O_{3(S)} + 2xSO_{2(g)} \quad (3)$$

$$2FeS_{2(S)} + 5.5O_{2(g)} \rightarrow Fe_2O_{3(S)} + 4SO_{2(g)} \quad (4)$$

The Debye-Scherer equation was used to determine the crystallite size, and Table 1 provided a summary of the result that was obtained. After an hour of calcination, the 35.98 nm crystallite size for chemical activation will decrease; this could be caused by the transformation of FeS_2 into hematite, and some S_2 will be released into the gas phase. However, this pigment was still made up of several metal oxides. As a result, larger crystallites are generated by longer calcination times. This result is lower than the hematite pigment's crystallite size as reported by Ismunandar et al. [22].

Table 1. The crystallite size of the treated pigment

Treatment	Crystallite size (nm)
Chemical activation	35.98
1 hour of calcination time	33.96
2 hours of calcination time	36.07
3 hours of calcination time	34.01

3.3. FTIR characterization of activated pyrite

The FTIR was carried out to determine the molecular vibration of activated pyrite. As shown in Figure 4, two peaks appear on spectra in the fingerprint area, meaning only inorganic components are contained in the sample, as explained by XRD and XRF results. The molecular vibration appear on 994 cm^{-1} was associated with the vibration from T–O–T bending; T can be composed of Si or Al element from aluminosilicate-backbone as another mineral deposited with pyrite. On the other hand, the molecular vibration on 483 cm^{-1} exhibited the presence of Si–O–Si and Fe–O as suitable with a previous study [23,20]. The molecular vibration result is summarized in Table 2.

Table 2. Molecular vibration of treated pyrite

Molecular vibration	Wavenumber (cm^{-1})
T—O—T (T = Si or Al)	994
Si—O—Si or Fe—O	483

3.4. Morphology of activated pyrite

The three-hour calcination period of physical activation process of pyrite as raw of inorganic pigment materials, the morphology of activated pyrite as pigment materials was examined using a field emission scanning electron microscope (FE-SEM). The pigment materials particles have an uneven form with rough particles, as seen in Figure 5. Additionally, the pigment particles agglomerated as a result of a solid-state reaction between more particles during the calcination process, which allows the surfaces of the particles to form the larger particles due to agglomeration.

The distribution of elements on the pigment material is also observed by the elemental mapping data via energy dispersive x-ray (EDX). As shown in Figure 6 and Figure 7, the dominant colors of green and yellow indicated the presence of silicon (Si) and iron (Fe) elements respectively, it was suitable to the XRF results depicted in Figure 1.
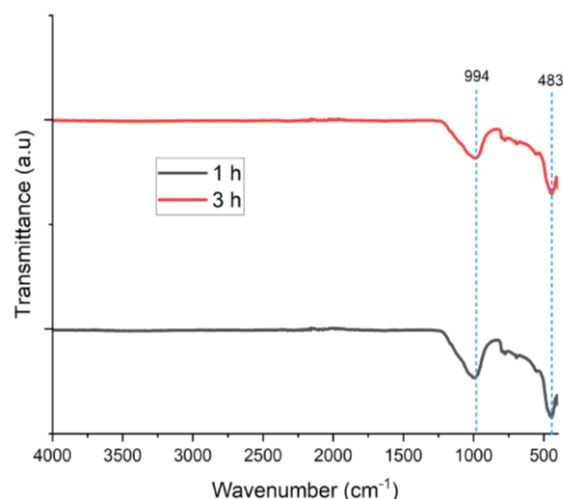

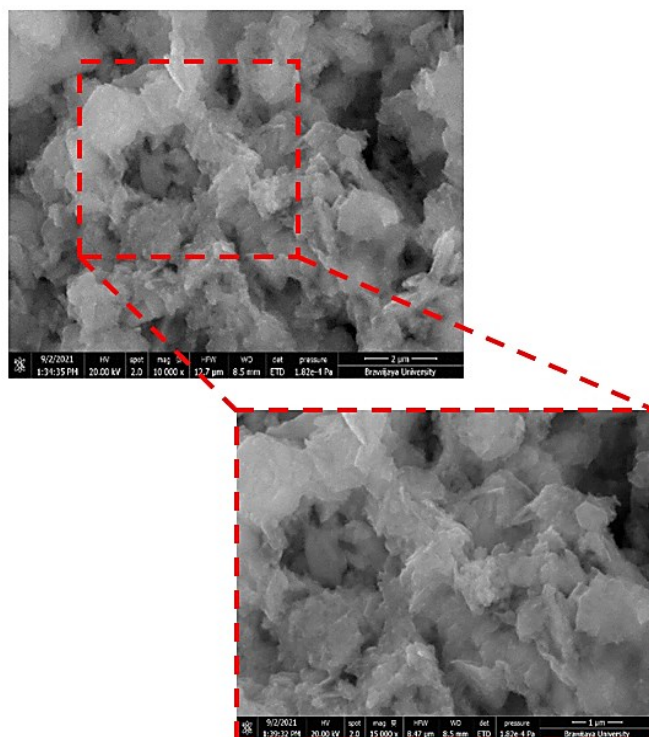Fig. 4. FTIR spectra of treated pyrite with calcination time of 1 and 3 hours

Fig. 5. Morphological structure of treated pyrite

In addition, the Al content was represented by the blue color, spread to practically every pigment area. While the Fe, in contrast to another compound, was evenly distributed over the entire region. Therefore, the production of the metal oxide is indicated by the presence of the oxygen element. It can be formed by the physical activation process of pyrite. Then it was suitable to the XRD data as introduced in Figure 2.
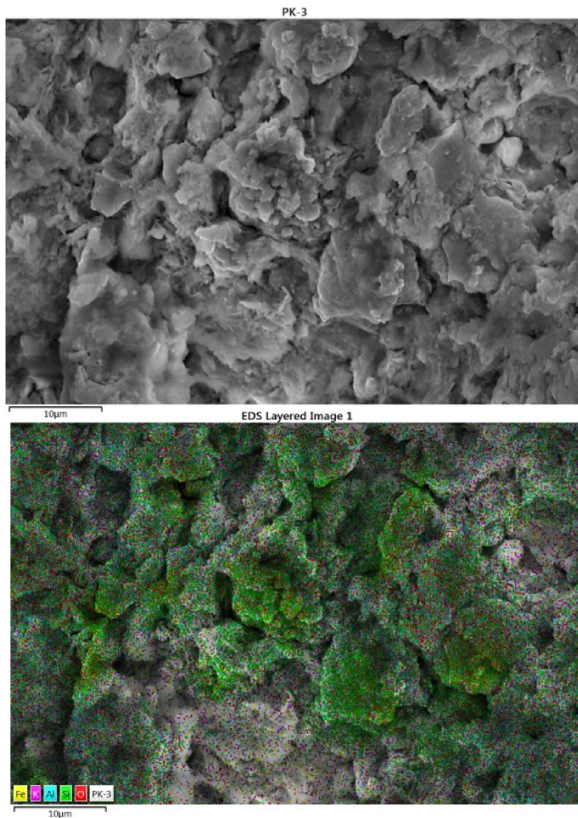
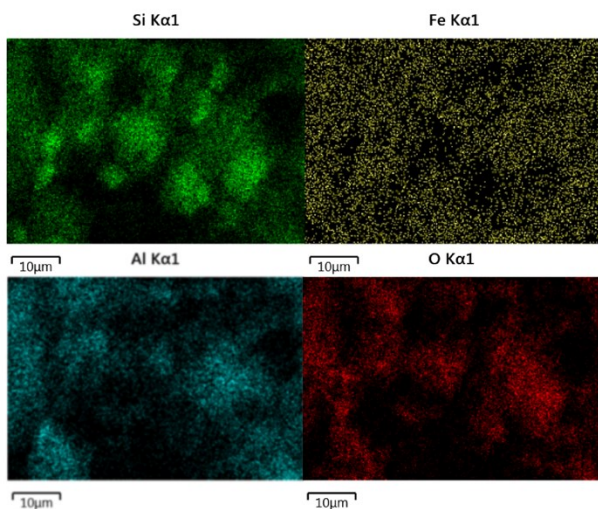Fig. 6. SEM micrograph and elemental mapping using EDX

Fig. 7. The distribution of each element is determined by EDX

The color of the inorganic pigment was determined by the chemical component. Hematite was reported as the main compound of red pigment. The color might be changed if it is deposited with another mineral or mixed with another component. Table 3 represents a comparison of this work and previous studies for red pigment development from natural mineral or industrial waste (sludge). As can be seen in Table 3, the higher purity of hematite leads to the formation of red pigment. On the other hand, if the hematite is mixed with another compound, like an aluminosilicate-based material, it will form a red-brown color. Then, the red mud, which was composed of 50% hematite and was treated using thermal treatment, led to brown pigment formation. It might be influenced by the presence of the gibbsite and goethite phases that lead to color transformation. Meanwhile, the natural pyrite

with chemical and physical activation obtained the red-brown pigment, a similar result reported by Lu et al. [24].

Table 3. Comparison with the previous study on red pigment

Natural Mineral/Waste	Pigment compound	Pigment color	References
Red mud with thermal treatment	α-Fe_2O_3, $FeO(OH)$, $Al(OH)_3$, $AlO(OH)$	Brown	[25]
Waste sludge from a zinc chloride production for synthesis of hematite pigment	α-Fe_2O_3	Red	[26]
Clay mineral as source of hematite red pigment synthesis	α-Fe_2O_3, kaolinite	Red-brown	[24]
Natural pyrite with chemical and physical activation treatment	Fe_2O_3, SiO_2, Al_2O_3	Red-brown	This work

4. Conclusion

Since iron manifests in the pyrite mineral as a reddish-brown color, it may be used as a possible source of inorganic pigment especially for red pigment. Based above finding, Fe is the highest element, occupying up to 42% of the overall, according to the XRF data. Then diffractogram of the pigment showed the presence of iron oxide phase, followed by the silica and alumina structures, as the main component that composed the inorganic pigment. Due to the heat exposure via physical activation process, the color of pigment was successfully transformed from gold to reddish-brown, which promising to be used for pigment application. Additionally, morphological observation shows the iron components are distributing throughout the entire pigmented area and the particles are aggregating. Lastly, the pyrite transformation into hematite-based inorganic pigment materials was promising pathways to produce low-cost pigment from an abundant natural resources through chemical and physical activation process.

References

[1]   A. Haris, B.D. Amin, A.M. Yusuf, Nurhasmi, Sintesis dan karakterisasi pyrite (FeS2) dari deposit mineral kecamatan Bontocani, kabupaten Bone, Sulawesi Selatan, JSPF, 10 (2014) 263-268.

[2]   R.M. Iqbal, E. Alyatikah, E.P. Toepak, R. Rasidah, L.R. Tambunan, S. Siswo, H. Fansuri, Chemical characteristic of fly ash from 3 Kalimantan's power plants as potential source for synthesis of aluminosilicate-based material, AIP Conf. Proc., 2349 (2021) 1-6.

[3]   R.M. Iqbal, W. Supriadi, R.Y.P. Burhan, S.D. Nurherdiana, R.E. Hidayati, S. Subaer, R. Bayuaji, H. Fansuri, Fabrication and characterization of fly ash-based geopolymer and its performance for immobilization of heavy metal cations, Communications in Science and Technology, 7 (2022) 112-118.

[4]   P. Venyite, J.G.D. Nemaleu, R.C. Kaze, A.B. Tchamba, E. Kamseu, U.C. Melo, C. Leonelli, Alkali-silica reactions in granite-based aggregates: The role of biotite and pyrite, Construction and Building Materials, 320 (2022) 126259.

[5]   M.L. Gomes, J.M. Klatt, G.J. Dick, S.L. Grim, K.I. Rico, M. Medina, W. Ziebis, L. Kinsman-Costello, N.D. Sheldon, D.A. Fike, Sedimentary pyrite sulfur isotope compositions preserve signatures of the surface microbial mat environment in sediments underlying low-oxygen cyanobacterial mats, Geobiology, 20 (2022) 60-78.

[6]   R.M. Iqbal, D.A.W. Pramoda, L. Hakim, A. Damsyik, R. Safitri, H.

Fansuri, The structural and optical band gap energy evaluation of TiO2-Fe2O3 composite, IOP Conf. Ser. Mater. Sci. Eng., 833 (2020).

[7]   D.A.P. Wardani, L. Rosmainar, R.M. Iqbal, S.N. Simarmata, Synthesis and characterization of magnetic adsorbent based on Fe2O3-fly ash from Pulang Pisau's power plant of Central Kalimantan, IOP Conf. Ser. Mater. Sci. Eng., 980 (2020).

[8]   A. Abrajevitch, B.J. Pillans, A.P. Roberts, K. Kodama, Magnetic properties and paleomagnetism of zebra rock, western australia: chemical remanence acquisition in hematite pigment and ediacaran geomagnetic field behavior, Geochem Geophys, 19 (2018) 732-748.

[9]   R.M. Iqbal, E.P. Toepak, D. Ayu, P. Wardani, Study of microstructure and optical properties of Fe2O3/TiO2 composites as functional materials, Jurnal Ilmiah Berkala: Sains dan Terapan Kimia, 16 (2022) 110-116.

[10] R.M. Iqbal, S.D Nurherdiana, D. Hartanto, M.H.D. Othman, H. Fansuri, Morphological control of La0.7Sr0.3Co0.2Fe0.8O3-δ and La0.7Sr0.3MnO3-δ catalytic membrane using PEG-H2O additive, IOP Conf. Ser. Mater. Sci. Eng., 348 (2018) 0-8.

[11] R.M. Iqbal, S.D. Nurherdiana, M.S. Sahasrikirana, L. Harmelia, W.P. Utomo, E.P. Setyaningsih, H. Fansuri, The compatibility of NiO, CeO2, and NiO-CeO2 as a coating on La0.6Sr0.4Co0.2Fe0.8O3-δ, La0.7Sr0.3Co0.2Fe0.8O3-δ and La0.7Sr0.3Mn0.3O3-δ ceramic membranes and their mechanical properties, IOP Conf. Ser. Mater. Sci. Eng., 367 (2018), 0-7.

[12] S.D. Nurherdiana, R. Etriana, R.M. Iqbal, W.P. Utomo, H. Fansuri, Effect of the sintering prcess on the morphology and mechanical properties of La0.6Sr0.4Co0.2Fe0.8O3-δ Asymmetric flat membranes prepared by the phase inversion method, Ceram. - Silik., 63 (2019) 305-314.

[13] S.D. Nurherdiana, S. Nikmatin, R.M. Iqbal, S.S. Mutya, P.U. Wahyu, A. Syafir, Nurlina, F. Hamzah, Preparation of La0.7Sr0.3Co0.2Fe0.8O3-δ (LSCF 7328) by combination of mechanochemical and solid state reaction, Key Engineering Materials, 744 (2017) 399-403.

[14] W.P. Utomo, A.S. Wijayanti, S.D. Nurherdiana, R.M. Iqbal, D. Hartanto, H. Fansuri, Preparation and morphological property of Co3O4/BaxSr1-xCo0.8Fe0.2O3-δ (x=0.5-0.7) membranes using starch as binder agent, IOP Conf. Ser. Mater. Sci. Eng., 588 (2019) 0-11.

[15] L. He, Z. Yue, C. Chen, C. Li, J. Li, Z. Sun, Enhancing iron uptake and alleviating iron toxicity in wheat by plant growth-promoting bacteria: theories and practices, IJAB, 23 (2020) 190-196.

[16] K. Tamura, T. Kunoh, N. Nagaoka, J. Takada, High-quality inorganic red pigment prepared by aluminum deposition on biogenous iron oxide sheaths, ACS Appl. Bio Mater., 3 (2020) 5699–5707.

[17] R. Zhang, L. Yang, R. Tu, J. Hui, J. Wang, J. Zhou, D. Chen, Emulsion phase inversion from oil-in-water (1) to water-in-oil to oil-in-water (2) induced by in situ surface activation of CaCO3 nanoparticles via adsorption of sodium stearate, Colloids Surf. A: Physicochem. Eng. Asp., 477 (2015) 55-62.

[18] I.M. Joni, L. Nulhakim, M. Vanitha, C. Panatarani, Characteristics of crystalline silica (SiO2) particles prepared by simple solution method using sodium silicate (Na2SiO3) precursor, J. Phys. Conf., 1080 (2018).

[19] Z.G. Eticha, R.E. Rojas-Hernandez, F.E. Olu, A. Yimam, I. Hussainova, E. Alemayehu, Effect of annealing temperature of brownish-red pigment based on iron oxide extracted by hydrothermal route from mill-scale steel slag, J. Sustain. Met., 8 (2022) 218-227.

[20] S. Sadasivam, H.R. Thomas, Colour and toxic characteristics of metakaolinite-hematite pigment for integrally coloured concrete, prepared from iron oxide recovered from a water treatment plant of an abandoned coal mine, J. Solid State Chem., 239 (2016) 246-250.

[21] H. Li, Y. Liu, Y. Liu, Q. Zeng, K. Hu, Z. Lu, J. Liang, Effect of sintering temperature in argon atmosphere on microstructure and properties of 3D printed alumina ceramic cores, J. Adv. Ceramics., 9 (2020) 220-231.

[22] Ismunandar, N. Nurdini, M.M. Ilmi, E. Maryanti, G.T.M. Kadja, Investigation on the crystal structures of hematite pigments at different sintering temperatures, Key Engineering Materials, 874 (2021) , 20–27.

[23] M. Hosseini-zori, E. Taheri-nassaj, A.R. Mirhabibi, Effective factors on synthesis of the hematite–silica red inclusion pigment, Ceram. Int., 34 (2008) 491-496.

[24] Y. Lu, W. Dong, W. Wang, J. Ding, Q. Wang, A. Hui, A. Wang, Optimal synthesis of environment-friendly iron red pigment from natural nanostructured clay minerals, Nanomaterials, 8 (2018).

[25] J. Carneiro, D.M. Tobaldi, W. Hajjaji, M.N. Capela, R.M. Novais, M.P. Seabra, J.A. Labrincha, Red mud as a substitute coloring agent for the hematite pigment, Ceram. Int., 44 (2018) 4211-4219.

[26] H. Ovcacikova, M. Velicka, P. Maierova, J. Vlcek, J. Tokarsky, T. Cegan, Characterization of waste sludge pigment from production of ZnCl2, Minerals, 11 (2021) 1-17.